AIAA 98-3698

Implications of Unsteady Analytical Flowfields on Rocket Combustion Stability

Joseph Majdalani
Marquette University
Milwaukee, WI 53233

Gary Flandro
Center for Advanced Space Propulsion
University of Tennessee Space Institute
Tullahoma, TN 37388

Tae-Seong Roh
California Institute of Technology
Pasadena, CA 91125

34th AIAA/ASME/SAE/ASEE
Joint Propulsion Conference & Exhibit
July 13 - 15, 1998 / Cleveland, OH

Implications of Unsteady Analytical Flowfields On Rocket Combustion Stability

J. Majdalani*
Marquette University, Milwaukee, WI 53233
G. A. Flandro†
University of Tennessee Space Institute, Tullahoma, TN 37388
T. S. Roh‡
California Institute of Technology, Pasadena, CA 91125

In the combustion stability assessment of solid propellant rocket motors, several new destabilizing terms are introduced when rotational flow effects are properly accounted for. Such effects must be included when the wave motion is parallel to the burning surface. A normal fluctuating velocity component then appears in a careful resolution of intrinsic fluid dynamics, including acoustico-vortical interactions that must satisfy mass and momentum conservation principles while accommodating the no-slip condition at the propellant surface. The source of this destabilizing term appears explicitly in two separate, independently derived, analytical formulations of the internal flowfield. Predictions generated by these analytical models are shown to agree with reliable computational data produced recently by a numerical code that solves the unsteady nonlinear Navier-Stokes equations. Verification of the analytical formulations by means of theoretical considerations, numerical comparisons, and global error assessments are also undertaken before examining the impact of the new time-dependent radial velocity correction on rocket stability. The new radial velocity fluctuations introduce a correction comparable in importance to the classical pressure coupling at the propellant surface. This effect along with several companion terms must be accounted for in the assessment of motor stability characteristics.

I. Introduction

In combustion stability assessments of solid rocket motors, the source of radial velocity fluctuations is frequently attributed to pressure oscillations at the propellant surface which, through the pressure coupling mechanism, viz., $\dot{m} \sim p^n$, can induce an oscillatory component in the radial direction. This is done without considering certain fluid dynamical interactions within the motor. In particular, effects related to the production of unsteady vorticity are lost in the assumption that the unsteady flow is a perturbed acoustic wave, and hence irrotational. This drawback is removed in two multidimensional formulations of the time-dependent field which correctly satisfy applicable conservation laws. As derived independently by Flandro[1] using regular perturbations, and Majdalani and Van Moorhem[2] using multiple scale expansions, two explicit formulations for the time-dependent field are now available that satisfy all appropriate conservation principles. In addition to satisfying applicable laws of physics, these expressions agree very well with computational predictions obtained from full, compressible, nonlinearized, Navier-Stokes solvers.[3]

An important consequence of introducing the unsteady rotational flow corrections is the appearance of new terms in the stability assessment of the chamber.[1] One of these is a radial velocity fluctuation with an amplitude proportional to the mean flow Mach number. Hence, it has the same importance in the system stability as the pressure coupling effect, which has similar influence. In this paper we demonstrate that this term arises in two separate formulations of the problem. A careful numerical verification is also undertaken, so that any doubts regarding its origin can be resolved. This article begins by reviewing briefly in Sec. II the two distinct analytical formulations of the unsteady rotational flow in a rocket chamber. Since the correctness of either model depends largely on how accurately it can replicate reality, a careful verification

*Assistant Professor, Department of Mechanical and Industrial Engineering. Member AIAA.
†Boling Chair Professor of Mechanical and Aerospace Engineering. Associate Fellow, AIAA.
‡Post-Doctoral Scholar, Mechanical Engineering and Jet Propulsion Center. Member AIAA.

process is undertaken in Sec. III. This verification is threefold and includes theoretical, computational, and global error validations. The theoretical verification consists of insuring that flowfield components satisfy continuity. Computational validations involve thorough comparisons to recently acquired CFD data from a nonlinear Navier-Stokes solver. These comparisons illustrate the remarkable agreement between analytical and computational results. The global or total error that accompanies each individual formulation is carefully determined in addition to the order associated with each method. Having established with certainty the reported accuracy, Sec. IV focuses on a key flowfield component that produces a destabilizing effect of the same order of magnitude as the pressue coupling. The characteristics of this radial velocity fluctuation are described, emphasizing the nonzero value it assumes at the propellant surface (edge of the combustion zone). The direct impact on stability is covered in Sec V.

II. Analytical Models

Following Flandro's nomenclature,[4] the total velocity is expressed in two-dimensional axisymmetric coordinates after normalizing by the speed of sound:

$$\boldsymbol{u}(r,z,t) = M_b \boldsymbol{U}(r,z) + \varepsilon \boldsymbol{u}^{(1)}(r,z,t) \tag{1}$$

where $\boldsymbol{U}(r,z)$ denotes Culick's well-known mean flow profile,[5] M_b is the injection Mach number at the wall, and $\varepsilon = A_p/(\gamma p_0)$ is the normalized pressure-wave amplitude representing the primary perturbation parameter used to linearize the Navier-Stokes equations. From the axial and normal components of the velocity, the total unsteady component is

$$\boldsymbol{u}^{(1)}(r,z,t) = u_r^{(1)}\boldsymbol{e}_r + u_z^{(1)}\boldsymbol{e}_z \tag{2}$$

A. Regular Perturbation (RP) Formulation

Since the details of the derivation are presented in separate papers,[1,4] the goal now is to focus on the results. The time-dependent expressions for the velocity field are repeated here for the reader's convenience, as originally published:

$$u_z^{(1)}(r,z,t) = \sin(k_m z)\sin(k_m t) + (B^r \sin\varphi_0 - B^i \cos\varphi_0) r \exp(\phi^r)\sin(k_m z \sin\theta) \tag{3}$$

$$u_r^{(1)}(r,z,t) = M_b r^2 U_r^2 (B^r \cos\varphi_0 + B^i \sin\varphi_0) \times \exp(\phi^r)\cos(k_m z \sin\theta) \tag{4}$$

where

$$\xi = \omega_0^2 R \nu_0 / V_b^3,\ \theta = \frac{\pi}{2} r^2,\ U_r = -r^{-1}\sin\theta \tag{5}$$

$$\varphi_o = k_m t + \frac{S}{\pi}\ln\tan\left(\frac{\theta}{2}\right) \tag{6}$$

$$\phi^r = \frac{-\xi}{\pi^2}\left[\left(\frac{2\pi^2}{S^2} - 1\right) I(x) + \csc\theta + \frac{\pi}{2}\frac{\cos\theta}{U_r^2}\right] \tag{7}$$

$$I(x) \cong x + \frac{1}{18}x^3 + \frac{7}{1800}x^5 + \frac{31}{105840}x^7 + \ldots \tag{8}$$

$$C^r = \frac{(S^2+\xi)S^3 \exp\left[-\phi^r(1)\right]}{(S^2+\xi)^2 + \xi^2 S^2} \tag{9}$$

$$C^i = \frac{\xi S^4 \exp\left[-\phi^r(1)\right]}{(S^2+\xi)^2 + \xi^2 S^2} \tag{10}$$

$$B^r = C^r \frac{U_r}{S} + C^i \frac{\xi}{S^2 U_r},\ B^i = C^i \frac{U_r}{S} - C^r \frac{\xi}{S^2 U_r} \tag{11}$$

$$\phi^r(1) = \xi\left(0.0842922527 - 3.66386237665/S^2\right) \tag{12}$$

These results are accurate to $O(1/S)$, the reciprocal of the Strouhal number ($S = \omega_0 R/V_b$), which is always smaller than about 10% since $S > 10$. The global error thus decreases at higher oscillation frequencies, larger effective radii, and smaller injection speeds. It approaches the exact solution at higher oscillation modes, which are very difficult to resolve numerically.

A shorter version of the RP solution can be extruded at the expense of a loss in accuracy that is insignificant at high kinetic Reynolds numbers. The outcome consisting of

$$u_z^{(1)}(r,z,t) = \sin(k_m z)\sin(k_m t) + rU_r \exp(\phi^r)\sin\varphi_o \sin(k_m z \sin\theta) \tag{13}$$

$$u_r^{(1)}(r,z,t) = M_b r^2 U_r^3 \exp(\phi^r)\cos\varphi_o \cos(k_m z \sin\theta) \tag{14}$$

carries a maximum error bound of 18% for $Re_k = 5\times 10^5$ and $S = 100$. The order of the error associated with Eqs. (13)-(14) approaches $1/S$ asymptotically as $Re_k \to \infty$.

B. Multiple Scale (MS) Formulation

Based on a two-variable derivative expansion procedure, an alternative solution is furnished by Majdalani and Van Moorhem:[2]

$$u_z^{(1)}(r,z,t) = \sin(k_m z)\sin(k_m t) + rU_r \sin(k_m z \sin\theta)\exp(\zeta)\sin\varphi_0 \tag{15}$$

$$u_r^{(1)}(r,z,t) = M_b r^2 U_r^3 \cos(k_m z \sin\theta)\cos\varphi_0 \exp(\zeta) \tag{16}$$

where the spatial damping term $\zeta = \xi\eta U_r^{-3}$ is based on an effective scale function that controls the solution:

$$\eta = y\left[1 + cy^c\left(yr^{-1} - c\ln r\right)\right]^{-1};\ y = 1 - r;\ c = 3/2 \quad (17)$$

Note that the global error associated with Eqs. (15)-(16) is of $O(1/Re_k) \equiv O(\nu_0\omega_0^{-1}R^{-2})$. The latter is a very small quantity, independent of the injection speed, being the square of the ratio of the thin hard wall Stokes layer ($\sqrt{\nu_0/\omega_0}$), and the chamber radius. The error thus decreases at higher oscillation modes and larger radii. By comparison to the Strouhal number, the kinetic Reynolds number is a much larger quantity since, independently of ω_0, the ratio

$$\frac{Re_k}{S} = \frac{\omega_0 R^2/\nu_0}{\omega_0 R/V_b} = \frac{V_b R}{\nu_0} >> 1 \quad (18)$$

results in the classic injection Reynolds number, which is always significant. From a practical standpoint, the global errors associated with both models remain too small to affect the overall assessment by an appreciable amount. This will be confirmed in the forthcoming assessments.

III. Verifications

In order to establish irrefutably the accuracy reported in the previous section, we undertake analytical and computational verifications along with a careful error analysis to ascertain the order of the global error associated with both analytical formulations.

A. Analytical Verification

From mass conservation, both steady and time-dependent components of the total velocity must satisfy continuity. Since the steady function $\boldsymbol{U}(r,z)$ is clearly solenoidal (i.e., divergence-free), it is only natural to expect $\boldsymbol{u}^{(1)}(r,z,t)$ to be solenoidal as well. Indeed, one can easily show that both Eqs. (3)-(4) and Eqs. (15)-(16) satisfy, in the leading order terms, the continuity equation written in cylindrical coordinates, namely,

$$\nabla.\boldsymbol{u}^{(1)} = \frac{\partial u_r^{(1)}}{\partial r} + \frac{u_r^{(1)}}{r} + \frac{\partial u_z^{(1)}}{\partial z} = 0 \quad (19)$$

B. Computational (CFD) Verification

In previous work,[2,3] the analytical derivations mentioned above were found to concur, as they should, with the numerical solution of their governing, *linearized* Navier-Stokes equations. A recent comparison with computational data acquired from a full, *nonlinearized*, Navier-Stokes solver developed by Roh and co-workers,[6,7] shows remarkable agreement between analytical and computational predictions.

Comparisons are shown in Fig. 1 for a typical case at the first two oscillation modes. The physical parameters correspond to an average tactical rocket motor proposed by Flandro.[1] Additional test parameters include a chamber pressure of 5.066×10^6 Nm^{-2} (50 atm), a density of 6.586 kgm^{-3}, a kinematic viscosity of 7.69×10^{-6} m^{2}s^{-1}, a temperature of 2000 K, a ratio of specific heats of 1.3, a Prandtl number of 0.9, a speed

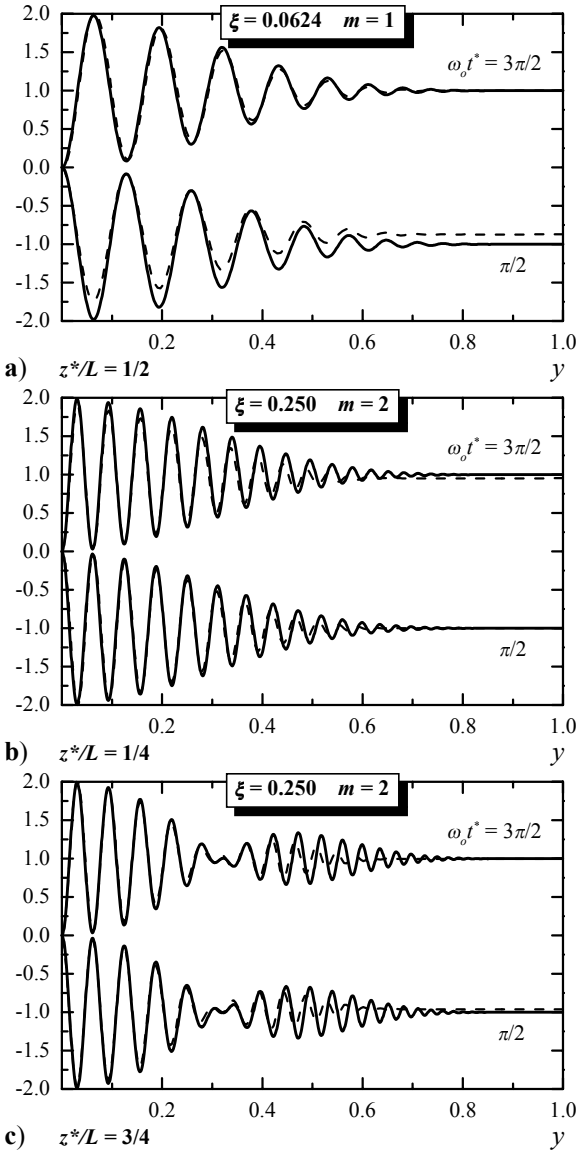

Fig. 1 Unsteady axial velocity obtained analytically (continuous lines) and from Navier-Stokes solvers (discontinuous lines) overlaid at two evenly spaced times in a typical tactical rocket motor. Results are for the first two oscillation modes evaluated at the first and last acoustic pressure nodes.

of sound of 1000 ms^{-1}, and an injection speed of 3 ms^{-1}. The CFD scheme employs a grid system that includes 60×150 nodes (in the axial and radial directions, respectively) for mode 1, and 80×240 nodes for mode 2, with a clustering ratio that increases with distance from the wall. This is necessitated by the need to resolve rapid variations that occur away from the wall as the spatial wavelength of vortical waves diminishes, being a direct function of Culick's radial velocity.[3] Since the spatial wavelength vanishes asymptotically as the centerline is approached, an increasingly larger number of nodes will be needed to maintain a uniform numerical error. A highly refined grid quickly becomes unaffordable due to increased memory requirements and CPU time.

In Fig. 1, the expected build-up in numerical error as the centerline is approached is attributed to the rough grid resolution used to generate the CFD data. This slight discrepancy, owing to unavoidable numerical errors, does not undermine the remarkable agreement with analytical predictions.

Another contribution to such deviations can be attributed to the finite time discretization used in the numerical scheme which allows producing CFD data at approximate times. While analytical predictions are shown at two instants separated by a phase difference that is exactly equal to π, (which happens to be an irrational number), numerical predictions are furnished at approximate phase differences.

Overall, within computational uncertainty, the CFD data indicates that, when turbulence is suppressed, the analytical models do represent the true nature of the internal flowfield. Representative data sets used to generate one time evolution in Fig. 1a are listed in Table 1 for confirmatory purposes.

C. Absolute Error Verification

In a recent paper on applied mathematics, Bosely[8] describes a rigorous technique that can be employed to verify categorically the error associated with an asymptotic solution. His technique serves two purposes: (1) to evaluate the order of the error, and (2) to ensure that the final expression is free from human errors. His technique is used here to verify the error associated with both regular perturbation and multiple scale formulations, in the hope of dispelling any possible doubts regarding the declared accuracy reported in the previous paragraphs.

Table 1 Unsteady axial velocity predictions

y	RP	MS	CFD
1.0	1.00000	1.00000	1.00000
0.9	1.00020	1.00020	1.00073
0.8	0.99560	0.99584	1.00069
0.7	0.98662	0.98858	0.99667
0.6	1.04700	1.04160	1.02463
0.5	0.89730	0.88565	0.90050
0.4	0.86056	0.83989	0.82500
0.3	1.30870	1.28400	1.19759
0.2	1.77650	1.78480	1.79982
0.1	0.80323	0.82064	0.83152
0.0	5.00E-5	6.3E-12	0.00688

The way this technique works is quite straightforward. We start by calculating the maximum absolute error, defined as the absolute difference between analytical and numerical solutions:

$$E_{\max} = \max_{0\le r\le 1} \left| u^{(1)}_{\text{numeric}} - u^{(1)}_{\text{analytic}} \right| \tag{20}$$

Then if $E_{\max}$ is of $O(1/S)$, as determined theoretically for the regular perturbation solution, one can write

$$E_{\max} = K(1/S)^{\alpha} \tag{21}$$

and show that $\alpha \to 1$ for large S. The order of the error can be determined from the slope of $E_{\max}$ versus $1/S$ plotted on a log-log scale. This slope can be determined quite accurately by using, for instance, the method of least-squares.

If, on the other hand, $E_{\max}$ is of $O(1/Re_k)$, as predicted theoretically for the multiple scale formulation, then one would set

$$E_{\max} = K(1/Re_k)^{\alpha} \tag{22}$$

and show that $\alpha \to 1$ for large Re_k.

The maximum error is thus evaluated and shown in Fig. 2 for the regular perturbation (Fig. 2a) and multiple scale (Fig. 2b) formulations. For the regular perturbations case, the error decreases and its order approaches unity with large Strouhal and kinetic Reynolds numbers. It deteriorates for small Strouhal numbers. For the multiple scale formulation, the same occurs for decreasing Strouhal and increasing kinetic Reynolds numbers. In a sense, the errors from both models are complementary with respect to the Strouhal number. This is clearly shown in Fig. 3 where errors from both models are shown at discrete values of the Strouhal number. In the same vein, a typical comparison of maximum absolute errors obtained for a tactical rocket motor with an Re_k of 2.1×10^6 is furnished in Table 2 below.

IV. Nonzero Radial Fluctuations

In this section, we address the character of unsteady radial velocities obtained from both analytical models. Before addressing the influence of this velocity

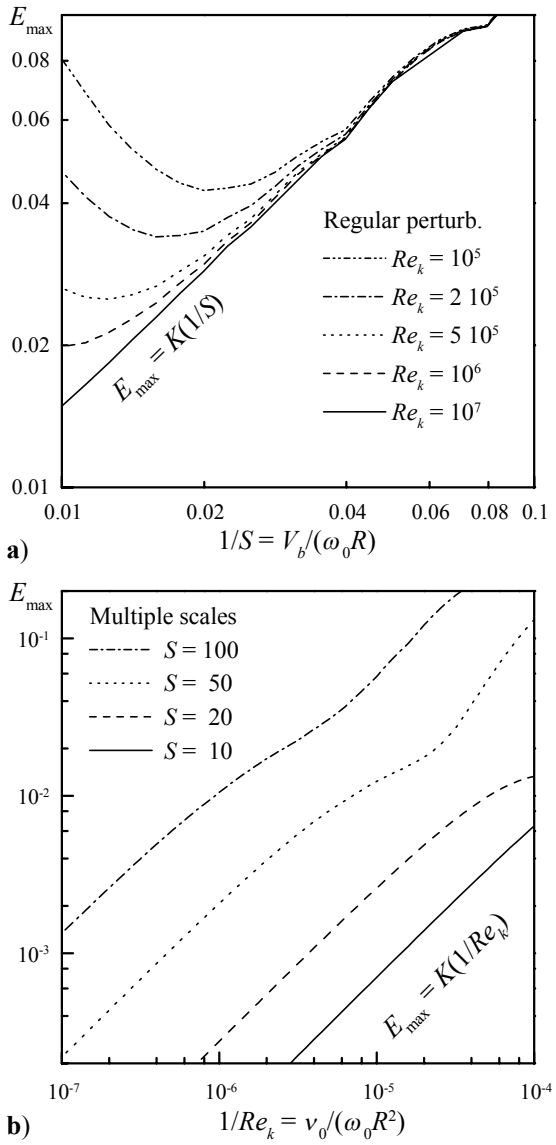

Fig. 2 Maximum absolute error associated with (a) Flandro's[1] regular perturbation and (b) Majdalani and Van Moorhem's multiple scale formulations.[2]

component on stability, we first undergo a comparative verification process to confirm the accuracy associated with both expicit formulations.

The explicit radial velocities expressed by Eq. (4) and Eq. (16), derived totally separately, are compared to each other, and to the corresponding numerical solution, for three cardinal cases reported in Ref. 1 that span a wide range of rocket motors. Without loss in generality, these comparisons are drawn in Fig. 4 for the first oscillation mode at $z^*/L = 15\%$ where the flowfield is predominantly laminar.

Clearly, both regular perturbation and multiple scale formulations coincide everywhere with the numerical solution. The same level of agreement persists at

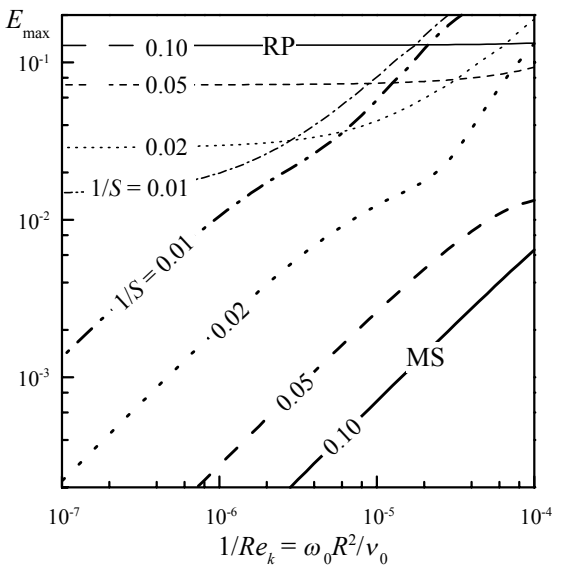

Fig. 3 Comparison of maximum absolute errors associated with Flandro's[1] and Majdalani and Van Moorhem's formulations.[2]

higher oscillation modes, and at different locations within the chamber (not shown here). The modulus of the rotational radial velocity expressed in complex notation, which is plotted in Fig. 4, is largest (in absolute value) at the wall, and decays as the centerline is approached. This is to be expected since the vorticity-coupled axial counterpart decays and vanishes when approaching the centerline as well. In particular, note that the nonzero value of the radial velocity at the wall negates traditional one-dimensional flowfield predictions which attribute velocity fluctuations to the pressure coupling response while ignoring internal flow interactions. This value for $u_r^{(1)}$ can be determined from either Eq. (4) or Eq. (16). The result is

$$u_r^{(1)}(1,z,t) = -M_b \cos(k_m z) = -M_b \cos(m\pi z^*/L) \quad (23)$$

Table 2 Maximum error for a tactical motor

$S = \frac{\omega_0 R}{V_b}$	RP	MS
10.000000	0.1285786	3.39398E-5
12.589258	0.0946560	5.61192E-5
15.848941	0.0876632	8.44848E-5
19.952633	0.0723662	1.31394E-4
25.118875	0.0547265	2.22025E-4
31.622753	0.0458222	3.54939E-4
39.810661	0.0359189	5.99515E-4
50.118782	0.0290877	0.0010290
63.095862	0.0236003	0.0017954
79.432534	0.0195297	0.0032031
100.00000	0.0167755	0.0057601

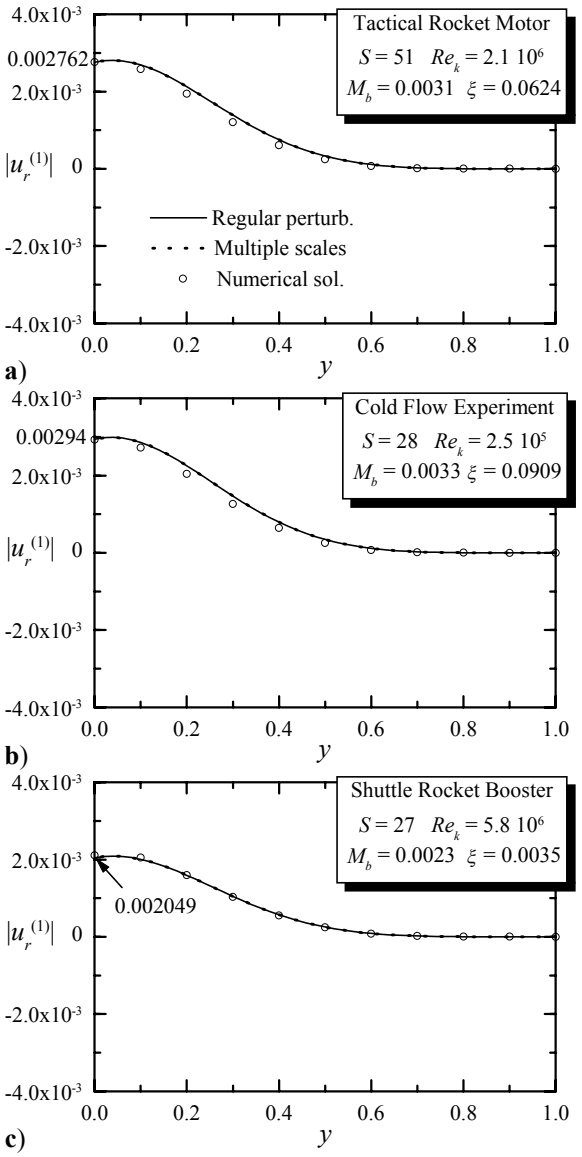

Fig. 4 Modulus of radial velocity fluctuations from both regular perturbation and multiple scale formulations compared with numerical predictions. Comparisons correspond to $m = 1$ and $z^*/L = 0.15$.

which, for $z^*/L = 15\%$, is $-0.891 M_b$. In Fig. 4, this value of the radial velocity amplitude at the wall is indicated for further emphasis. The graphical agreement shown in Fig. 4 is presented in tabular format for one case in Table 3 where data corresponding to the shuttle rocket booster are listed at 10 evenly spaced points. Note that the agreement with computational data is very good near the wall and deteriorates as we approach the centerline due to progressive build up in the numerical error for reasons already stated in Sec. III(B). The agreement between regular perturbation and multiple scale predictions is remarkable and includes, in some cases, matching digits up to the eighth decimal place.

Table 3 Unsteady radial velocity amplitudes (SRB)

y	RP	MS	Numerical
1.0	0.00000000	0.00000000	0.00000000
0.9	8.53137E-8	8.52946E-8	5.63200E-8
0.8	2.81421E-6	2.81590E-6	2.46140E-6
0.7	2.12909E-5	2.12990E-5	1.95797E-5
0.6	8.75767E-5	8.75969E-5	8.21043E-5
0.5	2.53138E-4	2.53175E-4	2.40537E-4
0.4	5.70289E-4	5.70344E-4	5.49830E-4
0.3	0.00104740	0.00104750	0.00102800
0.2	0.00159440	0.00159450	0.00159710
0.1	0.00200820	0.00200830	0.00204940
0.0	0.00204930	0.00204930	0.00210990

V. Stability Implications

Three different methods have been employed to determine the part of the radial velocity fluctuation that is created by the rotational flow corrections. In assessing the motor system stability characteristics, this radial velocity component must be added to others that arise in the irrotational (acoustic) part of the problem. In particular, terms that appear as a result of pressure sensitive combustion effects represent separate elements of the radial velocity fluctuation.

It should be apparent that the three separate calculations of the radial rotational velocity fluctuation are in substantial agreement. What is most important is that the predicted value of the radial velocity at the surface, $-M_b \cos(m\pi z^*/L)$, is proportional to the mean flow Mach number as already described. That is, it is of the same order of magnitude as other important parts of the system gain/loss balance. The velocity fluctuation is in phase with the pressure fluctuation. It therefore has the same significance as pressure coupling in the stability of the motor, since the response function is also proportional to the mean flow Mach number.

The new destabilizing term was discussed in detail in Reference 4, which also demonstrates that its inclusion improves the agreement between stability predictions and experimental data for motor systems that exhibit linear stability behavior.

VI. Concluding Remarks

What has been accomplished here is the verification that a new destabilizing term must be included in linear stability calculations for cases with wave motion parallel to the burning surfaces. The new findings are not the result of "double bookkeeping" as some critics contend. They represent natural gas motions that must be present when the no slip boundary conditions at the surfaces are accommodated. They arise in the same set of interactions that lead to the much discussed "flow turning" damping effect.

Acknowledgments

The authors wish to thank Professor Fred E. C. Culick from the California Institute of Technology and Professor Vigor Yang from the Pennsylvania State University for their helpful collaboration, constructive comments, and generous production of Navier-Stokes data that made comparisons to nonlinearized CFD predictions possible.

References

[1]Flandro, G. A., "On Flow Turning," AIAA Paper 95-2530, July 1995.

[2]Majdalani, J., and Van Moorhem, W. K., "Improved Time-Dependent Flowfield Solution for Solid Rocket Motors," *AIAA Journal,* Vol. 36, No. 2, 1998, pp. 241-248.

[3]Majdalani, J., "Characterization of the Laminar Boundary Layer in Solid Rocket Motors," AIAA Paper 98-3699, July 1998.

[4]Flandro, G. A., "Effects of Vorticity on Rocket Combustion Stability," *Journal of Propulsion and Power,* Vol. 11, No. 4, 1995, pp. 607-625.

[5]Culick, F. E. C., "Rotational Axisymmetric Mean Flow and Damping of Acoustic Waves in a Solid Propellant Rocket," *AIAA Journal,* Vol. 4, No. 8, 1966, pp. 1462-1464.

[6]Roh, T. S., Tseng, I. S., and Yang, V., "Effects of Acoustic Oscillations on Flame Dynamics of Homogeneous Propellants in Rocket Motors," *Journal of Propulsion and Power,* Vol. 11, No. 4, 1995, pp. 640-650.

[7]Roh, T. S., and Culick, F. E. C., "Transient Combustion Response of Homogeneous Propellants to Acoustic Oscillations in Axisymmetric Rocket Motors," AIAA Paper 97-3325, July 1995.

[8]Bosley, D. L., "A Technique for the Numerical Verification of Asymptotic Expansions," *SIAM Review,* Vol. 38, No. 1, 1996, pp. 128-135.